PCCP

Effect of branched versus linear alkyl side chains on the bulk heterojunction photovoltaic performance of small molecules containing both benzodithiophene and thienopyrroledione

Journal:	*Physical Chemistry Chemical Physics*
Manuscript ID:	CP-ART-01-2014-000077.R1
Article Type:	Paper
Date Submitted by the Author:	28-Feb-2014
Complete List of Authors:	Kim, Yu Jin; Postech, Park, Kwang Hun; GNU, materials Science & engineering Ha, Jong-jin; Gyung-sang national university, Polymer; GNU, materials Science & engineering Chung, Dae; Chung-Ang University, Chemical Engineering Kwon, Soon-Ki; GNU, materials Science & engineering Kim, Yun-Hi; Gyeongsang National University, Park, Chan; Pohang University of Science and Technology, Chemical Engineering

GRAPHICAL ABSTRACT

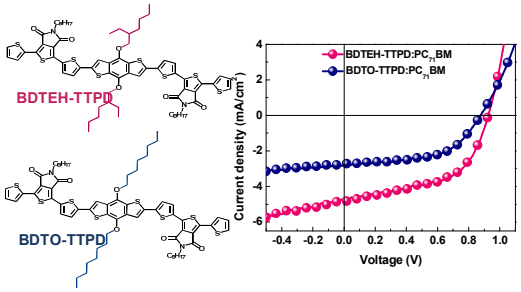

Compared to **BDTO-TTPD**, **BDTEH-TTPD** showed stronger light absorption, longer-range ordering, which results in higher power conversion efficiency.

Effect of branched versus linear alkyl side chains on the bulk heterojunction photovoltaic performance of small molecules containing both benzodithiophene and thienopyrroledione

Yu Jin Kim[a‡], Kwang Hun Park[b‡], Jong-jin Ha[b], Dae Sung Chung[d*], Soon-Ki Kwon[b*], Yun-Hi Kim[c*] and Chan Eon Park[a*]

[a] POSTECH Organic Electronics Laboratory, Department of Chemical Engineering, Pohang University of Science and Technology, Pohang, 790-784, Republic of Korea

[b] School of Materials Science & Engineering and Research Institute for Green Energy Convergence Technology (REGET), Gyeongsang National University, Jin-ju, 660-701, Republic of Korea

[c] Department of Chemistry & Research Institute of Natural Science, Gyeongsang National University, Jin-ju, 660-701, Republic of Korea

[d] School of Chemical Engineering and Material Science Chung-Ang University, Seoul, 156–756, Republic of Korea

*Corresponding Authors:

1. Prof. Chan Eon Park

POSTECH Organic Electronics Laboratory,

Department of Chemical Engineering,

Pohang University of Science and Technology,

Pohang, 790-784, Republic of Korea

Email: cep@postech.ac.kr

2. Prof. Soon-Ki Kwon

School of Materials Science & Engineering and Research Institute for Green Energy Convergence Technology (REGET),

Gyeongsang National University,

Jin-ju, 660-701, Republic of Korea

Email: skwon@gnu.ac.kr

3. Prof. Yun-Hi Kim

Department of Chemistry & Research Institute of Natural Science,

Gyeongsang National University,

Jin-ju, 660-701, Republic of Korea

Email: ykim@gnu.ac.kr

4. Prof. Dae Sung Chung

School of Chemical Engineering and Material Science,

Chung-Ang University

Seoul, 156–756, Republic of Korea

Email: dchung@cau.ac.kr

Correspondence to: Chan Eon Park (E-mail: cep@postech.ac.kr)

‡Yu Jin Kim and Kwang Hun Park contributed equally to this work.

Abstract

To evaluate the effect of side chain characteristics on the photovoltaic performance of small molecules containing both benzodithiophene (BDT) and thienopyrroledione (TPD), we designed and synthesized two such molecules, one containing a branched 2-ethylhexyl (2EH) side chain on the BDT unit (**BDTEH-TTPD**) and the other containing a linear *n*-octyl (C_8) side chain on the BDT unit (**BDTO-TTPD**). The optical and electrochemical properties and crystalline structures of these molecules were examined. Compared to **BDTO-TTPD**, **BDTEH-TTPD** showed stronger light absorption, longer-range ordering and shorter π-π stacking distances between backbones. As a result, the power conversion efficiency of a bulk heterojunction solar cell based on **BDTEH-TTPD** (2.40%) was substantially higher than that of the **BDTO-TTPD** device (1.12%).

Keywords

Small molecule, Benzodithiophene, Thienopyrroledione, Alkyl side chain, Organic solar cells, Power conversion efficiency

1. Introduction

In research on solar cell devices, solution processable small molecules have attracted interest as alternatives to polymers because they can be prepared with well-defined structures via simple synthetic processes in high purity.[1] Much progress has been made in the development of small molecule-based organic solar cells (SMOSCs), with power conversion efficiencies (PCEs) of up to 8% having been achieved.[2] Most SMOSCs developed to date, however, have low PCEs due to relatively low photocurrents arising from a narrow absorption range (< 700 nm) and disconnected donor matrix.[3] Thus, further research aimed at developing improved small molecule materials, especially in regard to molecular structure, design and engineering, is needed because such materials are key to achieving SMOSCs with high PCEs. Among the factors influencing SMOSC performance, the chemical structure of the small molecule donor has been shown to strongly influence properties such as light absorption[4], electronic compatibility with the acceptor molecule fullerene[5], charge transport characteristics[6], thin-film morphology[7], and molecular packing.[8] Varying the structure of the small molecule donor often has competing effects on these properties and hence on device performance. In particular, employing a longer solubilizing alkyl side chain generally improves solution-processability but simultaneously increases insulating content and reduces crystallinity in the solid state. Overcoming the performance limitations imposed by these competing effects requires a methodology that optimizes one property while having minimal adverse effects on other properties.

We recently synthesized a novel thieno[3,4-*c*]pyrrole-4,6-dione (TPD)-based small molecule.[9] From a materials standpoint, TPD is a promising organic semiconductor owing to its relatively simple, compact, symmetric, and planar structure that can potentially afford good electron delocalization in the solid state.[10] Enhanced performance (i.e., increased V_{OC} in OSCs) can be promoted by strong intra- and inter-chain interactions along and between

coplanar moieties as well as by the covalent introduction of electron-withdrawing groups to lower the HOMO and LUMO energy levels of the parent molecule.[11] In addition to the above, the simple introduction of different alkyl side chains on the pyrrole ring should also provide a means of modifying the solubility and processability of these materials.[12] Valuable insights into the design of TPD-based small molecules for use in functional devices was provided by the pioneering work of Zhan *et al,* who employed a TPD unit as the core acceptor moiety in SMOSCs.[13]

The benzo[1,2-b:4,5-b']dithiophene (BDT) unit, which consists of a fused benzene ring with two peripheral thiophene rings, is widely employed as an electron-donor in organic devices.[14] The extended π-system of the molecule induces strong intra- and intermolecular interactions in the solid state, thus benefiting charge transport in the devices.[15-16] According to these superior properties, Yang et al. reported a 10.1% PCE from acceptor-donor-acceptor (A-D-A) small molecule, SMPV1, comprised of BDT as the core unit and 3-octylrodanine as the electron-withdrawing end-group. Li and co- workers achieved a PCE of 6.75% from A-D-A structured small compounds, DO2, composed of BDT and indenedione unit.[16]

In the present study, we synthesized two small molecules, 3,3'-((4,8-bis((2-ethylhexyl)oxy)benzo[1,2-*b*:4,5-*b'*]dithiophene-2,6-diyl)bis(thiophene-5,2-diyl))bis(5-octyl-1-(thiophen-2-yl)-4H-thieno[3,4-*c*]pyrrole-4,6(5H)-dione (**BDTEH-TTPD**) and 3,3'-((4,8-bis(octyloxy)benzo[1,2-*b*:4,5-*b'*]dithiophene-2,6-diyl)bis(thiophene-5,2-diyl))bis(5-octyl-1-(thiophen-2-yl)-4H-thieno[3,4-*c*]pyrrole-4,6(5H)-dione (**BDTO-TTPD**) containing both novel BDT and TPD units (Scheme 1). We compared the optical and electrochemical properties, as well as the crystalline structures, of these compounds to examine the effects of the branched 2-ethylhexyl (2EH) side chains in **BDTEH-TTPD** versus the linear octyl alkyl side chains in **BDTO-TTPD**. The influence of the different side chains on OSC behavior was additionally examined.

2. Experimental

2.1. General Measurements and Instrumentation

^{1}H-NMR and ^{13}C-NMR spectra were recorded using Bruker Advance-300 and Bruker AM-200 spectrometers, respectively. HRMS (EI) spectra were collected using a high resolution GC mass spectrometer with LabRAM HR800 UV. MALDI-TOF/TOF spectra were recorded using a high resolution 4800 TOF/TOF mass spectrometer with Voyager DE-STR. Thermal gravimetric analysis (TGA) was performed on a TGA 2100 thermogravimetric analyzer (TA Instruments) using a heating rate of 10 °C/min. Differential scanning calorimetry (DSC) was conducted using a TA Instruments 2100 DSC with heating at 10 °C/min from 30 to 300 °C. Density functional theory (DFT) calculations were carried out at the B3LYP/6-31G* level of theory using the Spartan 08 computational programs. UV-Vis absorption spectra were recorded using a Cary 5000 UV-vis-near-IR double beam spectrophotometer. Photoluminescence (PL) spectra were obtained using a FP-6500 (JASCO). Cyclic voltammetry (CV) was performed using a PowerLab/AD instrument in 0.1 M solution of tetrabutylammonium hexafluorophosphate (Bu_4NPF_6) in anhydrous acetonitrile as a supporting electrolyte at a scan rate of 50 mV/s. A glassy carbon disk (~0.05 cm^2) coated with a thin small molecule film, an Ag/AgCl electrode, and a platinum wire were used as the working electrode, reference electrode, and counter electrode, respectively. Films of the synthesized small molecule alone and of small molecule:$PC_{71}BM$ blends were prepared on a Si/poly(3,4-ethlyenedioxythiophene) (PEDOT:PSS) substrate via spin-coating. These films were characterized using atomic force microscopy (AFM) and x-ray diffraction (XRD). AFM images were collected using a Multimode IIIa instrument (Digital Instruments) operated in tapping mode. XRD was performed using the 5A beamline (wavelength = 1.071 Å) at the Pohang Accelerator Laboratory (PAL) in Korea.

2.2. Device Fabrication and characterization

Solar cell devices were fabricated on an indium tin oxide-coated glass substrate with the following conventional structure: ITO-coated glass substrate / PEDOT:PSS / active layer (small molecule:PCBM) / LiF /Al. The ITO-coated glass substrate was first cleaned via sonication in detergent, deionized water, acetone, and isopropyl alcohol, with subsequent UV-Ozone treatment of the samples for 30 min. PEDOT:PSS (Baytron P VP AI 4083, filtered at 0.45 μm PVDF) was spin-cast from an aqueous solution to form a film of ca. 40 nm thickness. The substrate was dried for 10 min at 120 °C in air and then transferred into a glove box to spin-cast the active layer. Subsequently, the small molecule:PCBM active layer (ca. 100 nm) was spin-coated on the PEDOT:PSS layer at 1000 rpm from a homogeneously blended solution. Solutions containing a mixture of the small molecule and PCBM ($PC_{61}BM$ or $PC_{71}BM$) in chlorobenzene at a concentration of 40 mg/ml were prepared and then filtered through a 0.2 polytetrafluoroethylene (PTFE) filter prior to use. At the final stage, a LiF (1 nm) topped with aluminum (Al, 100 nm) electrode was deposited by thermal evaporation under vacuum at 2×10^{-6} torr. The current density-voltage (*J-V*) characteristics of the photovoltaic devices were measured under ambient conditions using a Keithley Model 2400 source-measurement unit. An Oriel xenon lamp (450 W) with an AM 1.5 G filter was used as the solar simulator. The light intensity was calibrated to 100 mW/cm^2 using a calibrated silicon cell with a KG5 filter, which is traced to the National Renewable Energy Laboratory (LREL). External quantum efficiency (EQE) spectra were obtained using a photomodulation spectroscopic set-up (model Merlin, Oriel) with a calibrated Si UV detector and a SR570 low noise current amplifier.

2.3. Hole mobility measurement

The hole only devices were fabricated with configuration of ITO/PEDOT:PSS/Small molecule or small molecule:$PC_{71}BM$/Au in an identical manner, except that a layer of 100 nm gold was deposited on the active thin film layer instead of the LiF/Al layer. The Au layer was deposited under a low speed (1 /s) to avoid the penetration of Au atoms into the active layer. Mobilities were extracted by fitting the current-voltage curves using the Mott-Curney relationship (space charge limited current).

$$J = \frac{9}{8}\varepsilon_0\varepsilon_r\mu_h\frac{V^2}{L^3}$$

Where J is the current density, L is the film thickness of active layer, μ_h is the hole mobility, ε_r is the relative dielectric constant of the transport medium, ε_0 is the permittivity of free space, V is the internal voltage in the device and $V = V_{appl} - V_r - V_{bi}$, where V_{appl} is the applied voltage to the device, V_r is the voltage drop due to contact resistance and series resistance across the electrodes, and V_{bi} is the built-in voltage due to the relative work function difference of the two electrodes. The V_{bi} can be determined from the transition between the ohmic region and the SCLC region.

3. Results and Discussion

3.1. Synthesis and thermal properties of the compounds

The two small molecules **BDTEH-TTPD** and **BDTO-TTPD** were synthesized according to the route shown in Scheme S1. Compounds 1–7 were prepared according to the literature.[17] Compound 7 was reacted with tributyltin-thiophene using $Pd(PPh_3)_2Cl_2$ as a catalyst in THF solvent, to afford compound 8 in 64% yield. Compound 8 was reacted with N-bromosuccinimide (NBS) in DMF/$CHCl_3$ solvent to afford compound 9 in 53% yield. Compounds 10 (**BDTEH-TTPD**) and 11 (**BDTO-TTPD**) were synthesized via Stille coupling reactions. **BDTEH-TTPD** was soluble in organic solvents (chloroform,

chlorobenzene, 1,2-dichlorobenzene) at room temperature whereas **BDTO-TTPD** was soluble in these solvents only at higher temperatures (60-100 °C).

In the fabrication of solution-processed solar cells, the thermal stability of the donor material is of crucial importance. Therefore, the thermal properties of **BDTEH-TTPD** and **BDTO-TTPD** were investigated by TGA and DSC (Figure 1). The TGA profiles showed decomposition temperatures (T_d, at 5% weight loss) of 390 °C for **BDTEH-TTPD** and 372 °C for **BDTO-TTPD** (Figure 1a and Table 1), indicating that both molecules have excellent thermal stability and are thus suitable for organic photovoltaic device applications. Interestingly, DSC (Figure 1b-c) showed that **BDTO-TTPD** exhibits a weak melting transition at 228 °C and crystallizes at 187 °C. By contrast, **BDTEH-TTPD**, which contains 2EH side chains, showed slightly higher melting and crystallization temperatures of 234 °C and 195 °C, respectively (Figure 1b). Also, the heats of melting and crystallization are both higher in **BDTEH-TTPD** compound than **BDTO-TTPD**. The higher melting temperature and melting enthalpy of **BDTEH-TTPD** compared to **BDTO-TTPD** is likely the result of a more planar structure.[18] In general, π-conjugated compounds appended with linear n-alkyl substituents show shorter π-π stacking distances as a result of lower steric hindrance relative to their branched alkyl substituted counterparts.[19] However, the branched side group (2EH) in our system showed higher crystallinity by closer intermolecular π-π interaction, which is possibly attributed to less steric hindrance and smaller torsional interactions than linear octyl group.

3.2. Theoretical calculations

Theoretical molecular orbital calculation was carried out at the B3LYP/6-31G* level of theory using the Spartan 08 computational programs to characterize optimized ground state geometry and electron density of HOMO and LUMO states. To simplify the calculation, alkyl

chains on TPD units are replaced by methyl groups. In optimized ground state geometry, **BDTEH-TTPD** showed more planar conformation due to small torsion angle between BDT and thiophene moiety than that of **BDTO-TTPD** (8.3° and 10.2° for **BDTEH-TTPD** and 28.8° and 30.1° for **BDTO-TTPD**) (Figure 2). The planar conformation due to the branched side group (2EH) is expected to the close-packing of the compounds, causing the π–π stacking distances of **BDTEH-TTPD** small molecule to decrease.[20] Also, the coplanarity facilitates efficient internal charge transfer between electron-donating BDT and electron-withdrawing TPD group. As the BDT moiety has a strong tendency for π–π stacking,[16] this structural planarity would synergetically reinforce the intermolecular interaction between neighboring molecules to give enhance transport property of **BDTEH-TTPD** compared to that of **BDTO-TTPD**.

3.3. Optical properties

The UV–visible absorption spectra of the small molecules were measured at room temperature both in solution (1×10^{-5} M in chlorobenzene) and in spin-cast thin films (Figure 3). The absorption data are summarized in Table 1. As shown in Figure 3a, the absorption spectra of **BDTEH-TTPD** and **BDTO-TTPD** in $CHCl_3$ show similar bands in the range of 350 to 600 nm, with a broad distinct peak at 450-600 nm arising from intramolecular charge-transfer (ICT) between the donor and acceptor moieties.[21] The shoulder peak observed from 350 to 450 nm can be attributed to the π-π* transitions of the conjugated molecular backbones.[22] Although both small molecules have the same backbone structure, the molar extinction coefficient (ε_{max}) of **BDTEH-TTPD** (33,260 L M^{-1} cm^{-1}) was larger than that of **BDTO-TTPD** (23,570 L M^{-1} cm^{-1}), indicating that **BDTEH-TTPD** has a greater capacity to absorb light.[23]

Figure 3b shows the absorption spectra of the spin-cast small molecule films. Compared to

the solution spectrum, each compound exhibits a bathochromic shift and broadening of the ICT band due to more effective donor–acceptor (D–A) interactions and extended π–π packing of the molecular backbones in the solid state.[24] The λ_{max} value of **BDTEH-TTPD** (566 nm) was red shifted compared to that of **BDTO-TTPD** (560 nm). This finding is consistent with the DSC and DFT analysis, whereby the branched alkyl chain of **BDTEH-TTPD** allows the molecule to adopt a planar structure, leading to stronger interactions, compared to the corresponding compound containing a linear alkyl chain. The energy band gaps calculated from the absorption band edges of the thin film spectra were determined to be 1.93 and 1.96 eV for **BDTEH-TTPD** and **BDTO-TTPD**, respectively. In terms of solar cell design, the smaller bandgap of **BDTEH-TTPD** will lead to higher photocurrent, making this molecule more useful for organic solar cell applications.[25]

PL spectra of spin-cast films of pure **BDTEH-TTPD** and **BDTO-TTPD**, and of 1:4 (w/w) blends of the small molecules and $PC_{71}BM$, were examined for their charge transfer properties (Figure 3c). **BDTEH-TTPD** showed a strong PL emission band with a maximum at 630 nm, whereas **BDTO-TTPD** exhibited a weak emission band at 639 nm, slightly red-shifted compared to that of **BDTEH-TTPD**. In the spectra of the blend films, the emission band for **BDTEH**:$PC_{71}BM$ was almost completely quenched compared with that of **BDTO-TTPD**:$PC_{71}BM$, indicating effective charge transfer between **BDTEH-TTPD** and $PC_{71}BM$ (i.e., more effective dissociation into separated charge carriers).[26]

3.4. Electrochemical properties and electron energy levels

Cyclic voltammetry was carried out using **BDTEH-TTPD** and **BDTO-TTPD** films on a Pt electrode at a scan rate of 50 mV/s, in order to determine the highest occupied molecular orbital (HOMO) energy levels of the compounds. Figure 4a shows the cyclic voltammograms of **BDTEH-TTPD** and **BDTO-TTPD** films. The onset oxidation potentials of **BDTEH-**

TTPD and **BDTO-TTPD** are 0.87 V and 0.93 V vs. Ag/AgCl, respectively (on the basis that ferrocene/ferrocenium is 4.8 eV below the vacuum level[27]). The corresponding HOMO energy levels were estimated to be -5.27 eV for **BDTEH-TTPD** and -5.33 eV for **BDTO-TTPD**, according to the equation: E_{HOMO} = -(E_{onset}^{ox} – $ferrocene_{onset}^{ox}$) - 4.8 eV, where $ferrocene_{onset}^{ox}$ is the onset oxidation potential of ferrocene (0.4 eV) as a reference.[28] The similarity of the HOMO energy levels of **BDTEH-TTPD** and **BDTO-TTPD**, which is in accordance with their oxidation potentials, demonstrates that the different alkyl chains incorporated into the molecules have only a minor effect on the electrochemical behavior of the compounds. The LUMO levels were determined to be -3.34 eV and -3.37 eV, respectively, using the calculated HOMO values and the optical band gaps. The values of the onset oxidation potential and HOMO and LUMO energy levels of the two compounds are listed in Table 2. The energy levels of the donor small molecules are very important for a high-performance photovoltaic device. First, the low-lying HOMO level of the small molecules can allow a high open-circuit voltage (Voc) for the photovoltaic cell, because the Voc is proportional to the energy difference between the HOMO level of the donor and the LUMO level of the acceptor. Second, the LUMO energy level of the donor has to be at least 0.3 eV higher than that of the acceptor (e.g., PCBM) to guarantee formation of a downhill driving force for the energetically favorable electron transfer reactions.[29] Certainly, **BDTEH-TTPD** and **BDTO-TTPD** presents relatively low HOMO energies ensured high V_{OC} (> 1.0 V), and well-aligned LUMO energies with that of PCBMs for efficient charge dissociation (Figure 4b).

3.5. Photovoltaic properties

To explore the photovoltaic performance of the small molecules, bulk heterojunction solar cells were fabricated using **BDTEH-TTPD** or **BDTO-TTPD** as the donor and a fullerene

derivative, $PC_{61}BM$ or $PC_{71}BM$, as the acceptor with the conventional device architecture ITO/PEDOT:PSS/**BDTEH-TTPD** or **BDTO-TTPD**:$PC_{61}BM$ or $PC_{71}BM$/LiF/Al. During the preliminary device optimization process, the effect of varying the **BDTEH-TTPD**:$PC_{61}BM$ or **BDTO-TTPD**:$PC_{61}BM$ active-layer compositions (from 1:1 to 1:4 w/w) was first investigated. The current density voltage (*J-V*) characteristics under one sun (simulated AM1.5G irradiation at 100 mW cm^{-2}) are shown in Figure 5 and the photovoltaic parameters collected are listed in Table 3. For both the **BDTEH-TTPD**:$PC_{61}BM$ and **BDTO-TTPD**:$PC_{61}BM$ blends, a weight ratio of 1:4 was found to give the best performance. The device with a 1:4 **BDTEH-TTPD**:$PC_{61}BM$ weight ratio had an open-circuit voltage (Voc) of 0.90 V, a short-circuit current (Jsc) of 3.0 mA cm^{-2}, and a fill factor (FF) of 61.1%, resulting in a PCE of 1.71%. In contrast, the **BDTO-TTPD**:$PC_{61}BM$ device with the same ratio showed slightly inferior performance, with a Voc of 0.87 V, Jsc of 2.3 mA cm^{-2}, and FF of 55.7%, yielding a PCE of 1.10%. Because **BDTEH-TTPD** and **BDTO-TTPD** have similar low-lying HOMO energy levels, they produced similar V_{OC} values in the solar cell devices.

$PC_{71}BM$ absorbs more strongly in the visible region than does $PC_{61}BM$.[30] Therefore, under identical device conditions, $PC_{71}BM$ would be expected to contribute more to the current from the device than $PC_{61}BM$, and may thus provide a means to enhance the device efficiency. To determine if the performances of the small molecules could be further improved using the acceptor $PC_{71}BM$, we fabricated a series of devices based on small molecule/$PC_{71}BM$ blends. The small molecule to $PC_{71}BM$ weight ratio was fixed at 1:4 and the active layer was coated from a chlorobenzene solution, as this condition was optimal for $PC_{71}BM$. The characteristics of the devices based on **BDTEH-TTPD**:$PC_{71}BM$ and **BDTO-TTPD**:$PC_{71}BM$ are also listed in Table 3. Changing the electron acceptor from $PC_{61}BM$ to $PC_{71}BM$ yielded a higher J_{SC} for both the **BDTEH-TTPD** and **BDTO-TTPD** devices, an improvement that can be attributed to the higher absorption coefficient of $PC_{71}BM$ in the

visible region. [31] Interestingly, the increase in J_{SC} for **BDTEH-TTPD** (from 3.0 to 4.7 mA cm^{-2}) was much larger than that for **BDTO-TTPD**. J_{SC} strongly depends on the number of generated excitons in the photoactive layers and photo-response (conversion of input photons to photocurrent) as well as on properties such as film morphology and nanostructural order. (Film morphology will be discussed below.) Although **BDTEH-TTPD** and **BDTO-TTPD** have a similar E_g with a gap difference of 0.03 eV, **BDTEH-TTPD** has a 1.41 times higher molar absorptivity than **BDTO-TTPD**, which likely contributed to greater exciton and charge generation in the **BDTEH-TTPD**:$PC_{71}BM$ device than in the **BDTO-TTPD**:$PC_{71}BM$ device. [32] Moreover, the photo-response of **BDTEH-TTPD** was over 40% at 418 nm, whereas that of **BDTO-TTPD** was over 25% at 420 nm (Figure 5d). The higher EQE spectrum of **BDTEH-TTPD** can be attributed to greater conversion of input photons to photocurrent at all absorption wavelengths, consistent with the higher circuit current observed.[33]

3.6. Thin-Film Morphology

The solubilizing side chains of **BDTEH-TTPD** and **BDTO-TTPD** are expected to impact their solubility and miscibility with PCBM, which may in turn affect the film morphology generated during spin-coating. AFM was used to investigate the nanoscale topography of the **BDTEH-TTPD**:$PC_{71}BM$ and **BDTO-TTPD**:$PC_{71}BM$ composite films with the same weight ratio (1:4 w/w) (Figure 6). The **BDTEH-TTPD**:$PC_{71}BM$ blend film displayed homogeneous clusters with many aggregated domains, with a root-mean-square (RMS) roughness of 1.07 nm (Figure 6a, c). By contrast, the blended **BDTO-TTPD**:$PC_{71}BM$ film exhibited a poor BHJ morphology (tough and chapped surface) with a smaller RMS roughness of 0.47 nm (Figure 6b, d). The larger roughness of the **BDTEH-TTPD**:$PC_{71}BM$ compared with the **BDTO-TTPD** blend film indicates a higher degree of order, which suggests that **BDTEH-TTPD**:$PC_{71}BM$ films would show reduced internal resistance and more efficient charge

separation in SMOSCs. A higher surface roughness and nanoscale texture will also lead to increased internal light scattering and enhanced light absorption.[34] All of these characteristics will contribute to the higher *J*sc value and efficiency of the **BDTEH-TTPD**:$PC_{71}BM$ device relative to the **BDTO-TTPD**:$PC_{71}BM$ device. The marked morphological differences between the **BDTEH-TTPD**:$PC_{71}BM$ and **BDTO-TTPD**:$PC_{71}BM$ films indicate that fine tuning of the molecular structure to achieve a desirable morphology in the solid state is critical to optimizing solar cell performance. The difference in PCE values is also influenced by properties such as film morphology and nanostructural order, which will be discussed below.

3.7. Thin-Film Nanostructural Order.

To determine the influence of the side-chain characteristics on the nanostructural order within the active layer, the XRD patterns (out-of-plane and in-plane) of the pure small molecule films and the blend films were measured (Figure 7). It is obvious from the patterns of small molecule-only films (Figure 7a, red lines) that the **BDTEH-TTPD** shows well ordered structure, contains a third order reflection as the lamellar (2θ = 3.91°) and π-π stacking (2θ = 17.05°) peaks appear in the out-of plane and in-plane pattern, respectively. The corresponding interlayer *d*-spacing and π-π intermolecular stacking distance were 15.69 Å and 3.61 Å, respectively. For the pure **BDTO-TTPD** film (blue lines), crystalline diffraction peaks (2θ = 3.55°, *d*-spacing = 17. 28 Å) and a π-π in-plane peak were observed but their intensities were weak and the third-order diffraction was absent, suggesting that the **BDTO-TTPD** film contains much less crystalline order.[35] These findings, which indicate that the **BDTEH-TTPD** film is comprised of higher order **BDTEH-TTPD** crystallites,[36] agree well with the DSC and UV-vis spectroscopy findings regarding the crystallinity. The higher crystallinity of **BDTEH-TTPD** can be attributed to its branched alkyl chains (2EH), which

provide less steric hindrance than the linear chain (C_8) in **BDTO-TTPD**.

For the small molecule:$PC_{71}BM$ blended films (1:4 w/w) (Figure 7b), the relative order in the out-of-plane and in-plane directions differed from that observed for the films composed of only the small molecule. The weaker and broad reflections observed for the blended films can be attributed to disruption of the crystalline packing by the presence of PCBM.[37] However, the diffraction patterns were similar for the pure and blended films, indicating that the same crystalline planes were present in each system. It should be noted that the XRD patterns for the **BDTEH-TTPD**:$PC_{71}BM$ film retained the signals indicative of a high-order crystalline plane observed in the patterns for the pure **BDTEH-TTPD** film. In addition, the **BDTO-TTPD**:$PC_{71}BM$ blended film showed very weak second diffraction peaks and π-π stacking diffraction in the out-of-plane and in-plane directions, respectively, indicating low crystallinity. The dominant long-range ordering and distinct π-π stacking of **BDTEH-TTPD** in the blend film allows efficient charge transport, which would explain, at least in part, why devices based on **BDTEH-TTPD** showed an almost two-fold higher PCE and superior performance compared to those based on the less ordered **BDTO-TTPD** structure.[38]

3.8. Hole mobility

To quantitatively investigate the effect of intermolecular packing on the charge transport property, hole mobility was evaluated using the space charge limited current (SCLC) model. The experimental details are described in the Experimental section. The hole mobility is measured in the dark using hole-only devices (ITO/PEDOT:PSS/small molecule or small molecule:$PC_{71}BM$/Au) and obtained from the slope of the plot log J_D vs. voltage (Figure 8). When the hole mobilities of pure small molecules are compared, it has been observed that the hole mobility of **BDTEH-TTPD** (8.76×10^{-5} cm^2 V^{-1} s^{-1}) is higher than that of the **BDTO-TTPD** (2.42×10^{-5} cm^2 V^{-1} s^{-1}). The enhancement of hole mobility for **BDTEH-TTPD** is

may arise from the denser packing of small molecules with branched alkyl chains (2EH), as evidenced from XRD patterns analysis. Likewise, higher hole mobility was also observed for the blends of **BDTEH-TTPD** and $PC_{71}BM$ compared with the blends of **BDTO-TTPD**:$PC_{71}BM$, 6.52×10^{-6} cm^2 V^{-1} s^{-1} vs 3.91×10^{-6} cm^2 V^{-1} s^{-1}. This result also indicates that the stronger intermolecular interaction of **BDTEH-TTPD** enables higher hole mobility in BHJ films. However, the hole mobilities of **BDTEH-TTPD**:$PC_{71}BM$ and **BDTO-TTPD**:$PC_{71}BM$ blends are decreased by 1 order of magnitude compared to that of pure small molecule. As mentioned above, this is probably because the disruption of the crystalline packing according to the presence of PCBM.

4. Conclusion

Two small molecules, **BDTEH-TTPD** and **BDTO-TTPD**, which both contain BDT and TPD but have branched and linear alkyl side chains, respectively, were synthesized and studied as potential materials for SMOSC applications. We investigated the effect of these different side chains on the optical, electrochemical, and solid-state packing properties and the resultant PCE of the fabricated OSC device. **BDTEH-TTPD**, which contains branched 2EH side chains, exhibited higher light absorption, a smaller band gap, and a more planar structure than **BDTO-TTPD**, which contains a linear side group (C_8). An OSC device incorporating **BDTEH-TTPD** exhibited a high V_{OC} of 0.92 V, J_{SC} of 4.7 mA / cm^2, FF of 54.4% and PCE of 2.40%, whereas a device based on **BDTO-TTPD** displayed a V_{OC} of 0.89 V, J_{SC} of 2.7 mA / cm^2, FF of 55.2% and PCE of 1.33%. The present findings highlight the importance of the alkyl side chains on BDT- and TPD-based small molecules to the performance of these materials in SMOSCs.

5. References

1 a) A. Mishra, P. Bäuerle, *Angew. Chem. Int. Ed*. 2012, **51**, 2020; b) Y. Sun, G. C. Welch, W. L. Leong, C. J. Takacs, G. C. Bazan, A. J. Heeger, *Nat. Mat*. 2011, **11**, 44; c) J. Zhou, X. Wan, Y. Liu, Y. Zuo, Z. Li, G. He, G. Long, W. Ni, C. Li, X. Su, Y. Chen, *J. Am. Chem. Soc*. 2012, **134**, 16345.

2 J. Zhou, Y. Zuo, X. Wan, G. Long, Q. Zhang, W. Ni, Y. Liu, Z. Li, G. He, C. Li, B. Kan, M. Li, Y. Chen, *J. Am. Chem. Soc*. 2013, **135**, 8484.

3 a) B. Walker, C. Kim, T. –Q. Nguyen, *Chem. Mater*. 2011, **23**, 470; b) Y. Lin, Y. Li, X. Zhan, *Chem. Soc. Rev*. 2012, **41**, 4245.

4 a) A.T. Yiu, P. M. Beaujuge, O. P. Lee, C. H. Woo, M. F. Toney, J. M. J. Frechet, *J. Am. Chem. Soc*. 2012, **134**, 2180; b) Y. Li, *Acc. Chem. Res*. 2012, **45**, 723.

5 a) I. Meager, R. S. Ashraf, S. Rossbauer, H. Bronstein, J. E. Donaghey, J. Marshall, B. C. Schroeder, M. Heeney, T. D. Anthopoulos, I. McCulloch, *Macromolecules*. 2013, **46**, 5961; b) P. A. Troshin, D. K. Susarova, E. A. Khakina, A. A. Goryachev, O. V. Borshchev, S. A. Ponomarenko, V. F. Razumov, N. S. Sariciftci, *J. Mater. Chem*. 2012, **22**, 18433.

6 A. Y. Chang, Y. -H. Chen, H. –W. Lin, L.-Y. Lin, K. –T. Wong, R. D. Schaller, *J. Am. Chem. Soc*. 2013, **135**, 8790.

7 a) J. A. Love, C. M. Proctor, J. Liu, C. J. Takacs, A. Sharenko, T. S. van der Poll , A. J. Heeger, G. C. Bazan, T. –Q. Nguyen, *Adv. Funct. Mater*. 2013; b) J. R. Tumbleston, A. C. Stuart, E. Gann, W. You, H. Ade, *Adv. Funct. Mater*. 2013, **23**, 3463.

8 N. C. Miller, E. Cho, R. Gysel1, C. Risko, V. Coropceanu, C. E. Miller, S. Sweetnam, A. Sellinger, M. Heeney, I. McCulloch, J. –L. Brédas, M. F. Toney, M. D. McGehee, *Adv. Mater*. 2012, **2**, E1208.

9 J. Ha, Y. J. Kim, J. Park, T. K. An, S. –K. Kwon, C. E. Park, Y. -H. Kim, *Chem. Asian J.* 2014, (online published)

10 Y. Zou, A. Najari, P. Berrouard, S. Beaupre´, B. R. Aich, Y. Tao, M. Leclerc, *J. Am. Chem. Soc*. 2010, **132**, 5330.

11 Y. -R. Hong, H. -K. Wong, L. C. H. Moh, H. -S. Tan, Z. -K. Chen, *Chem. Comm*. 2011, **47**, 4920.

12 T. –Y. Chu, J. Lu, S. Beaupré, Y. Zhang, J. –R. Pouliot, S. Wakim, J. Zhou, M. Leclerc, Z. Li , J. Ding , Y. Tao, *J. Am. Chem. Soc*. 2011, **133**, 4250.

13 Y. Lin, P. Cheng, Y. Liu, X. Zhao, D. Li, J. Tan, W. Hu, Y. Li, X. Zhan, *Sol. Energy Mater. Sol. Cells*. 2012, **99**, 301.

14 S. Shen, P. Jiang, C. He, J. Zhang, P. Shen, Y. Zhang, Y. Yi, Z. Zhang, Z. Li, Y. Li, *J. Am. Chem. Soc*. 2013, **25**, 2274.

15 a) J. Yuan, X. Huang, F. Zhang, J. Lu, Z. Zhai, C. Di, Z. Jiang, W. Ma, *J. Mater. Chem.* 2012, **22**, 22734; b) H. Zhou, L. Yang, A. C. Stuart, S. C. Price, S. Liu, W. You, *Angew. Chem. Int. Ed*. 2011, **123**, 3051.

16 a) Y. Liu, C. –C. Chen, Z. Hong, J. Gao, Y. Yang, H. Zhou, L. Dou, G. Li, Y. Yang, *Sci. Rep*. 2013, 3, 3356; b) S. Shen, P. Jiang, C. He, J. Zhang, P. Shen, Y. Zhang, Y. Yi, Z. Zhang, Z. Li, Y. Li, *Chem. Mater*. 2013, 25, 2274; c) Y. Liu , X. Wan, F. Wang, J. Zhou, G. Long, J. Tian, Y. Chen, *Adv. Mater*. 2011, 23, 5387.

17 a) C. B. Nielsen, T. Bjornholm, *Org. Lett.* 2004**, 6**, 3381; b) G. Sotgiu, M. Zambianchi, G. Barbarella, C. Botta, *Tetrahedron.* 2002, **58**, 2245; c) C. Cabanetos, A. E. Labban, J. A. Bartelt, J. D. Douglas, W. R. Mateker, J. M. J. Fréchet, M. D. McGehee, P. M. Beaujuge, *J. Am. Chem. Soc*. 2013, **135**, 4656; d) L. Huo, J. Hou, H. –Y. Chen, S. Zhang, Y. Jiang, T. L. Chen, Y. Yang, *Macromolecules*. 2009, **42**, 6564.

18 a) G. C. Welch, L. A. Perez, C. V. Hoven, Y. Zhang, X. –D. Dang, A. Sharenko, M. F. Toney, E. J. Kramer, T. –Q. Nguyen, G. C. Bazan, *J. Mater. Chem*. 2011, **21**, 12700; b) N. D. Eisenmenger, G. M. Su, G. C. Welch, C. J. Takacs, G. C. Bazan, E. J. Kramer, M. L.

Chabinyc, *Chem. Mater*. 2013, **25**, 1688; c) F. Liang, J. Lu, J. Ding, R. Movileanu, Y. Tao, *Macromolecules.* 2009, **42**, 6107.

19 A. T. Yiu, P. M. Beaujuge, O. P. Lee, C. H. Woo, M. F. Toney, J. M. J. Fréchet, *J. Am. Chem. Soc*. 2012, **134**, 2180.

20 Y. Lee, Y. M. Nam, W. H. Jo, *J. Mater. Chem*. 2011, **21**, 8583

21 Q. Peng, S. –L. Lim, I. H. –K. Wong, J. Xu, Z. –K. Chen, *Chem. Eur. J*. 2012, **18**, 12140.

22 Y. –Y. Lai, J. –M. Yeh, C. –E. Tsai, Y. –J. Cheng, *Eur. J. Org. Chem*. 2013, 5076.

23 Y. -X. Xu, C. –C. Chueh, H. –L. Yip, F. –Z. Ding, Y. –X. Li, C. –Z. Li, X. Li, W. –C. Chen, A. K.-Y. Jen, *Adv. Mater*. 2012, 24, 6356.

24 B. Walker, A. B. Tamayo, X. –D. Dang, P. Zalar, J. H. Seo, A. Garcia, M. Tantiwiwat, T. –Q. Nguyen, *Adv. Funct. Mater*. 2009, **19**, 3063.

25 H. Zhong, Z. Li, F. Deledalle, E. C. Fregoso, M. Shahid, Z. Fei, C. B. Nielsen, N. Y-Gross, S. Rossbauer, T. D. Anthopoulos , J. R. Durrant, M. Heeney, *J. Am. Chem. Soc*. 2013, **135**, 2040.

26 J. J. B-Smith, L. Goris, K. Vandewal, K. Haenen, J. V. Manca, D. Vanderzande, D. D. C. Bradley, J. Nelson, *Adv. Funct. Mater*. 2007, **17**, 451.

27 J. E. Coughlin, Z. B. Henson, G. C. Welch, G. C. Bazan, *Acc. Chem. Res*. 2013,

28 X. Yu, X. Jin, G. Tang, J. Zhou, W. Zhang, D. Peng, J. Hu, C. Zhong, *Eur. J. Org. Chem*. 2013, 5893.

29 a) T. –Y. Chu, J. Lu, S. Beaupré, Y. Zhang, J. –R. Pouliot, S. Wakim, J. Zhou, M. Leclerc, Z. Li, J. Ding, Y. Tao, *J. Am. Chem. Soc*. 2011, **133**, 12, 4250; b) H. Bürckstümmer, E. V. Tulyakova, M. Deppisch, M. R. Lenze, N. M. Kronenberg, M. Gsänger, M. Stolte, K. Meerholz, F. Würthner, *Angew. Chem. Int. Ed*. 2011, **123**, 11832.

30 P. Dutta, W. Yang, S. H, Eom, S. –H. Lee, *Org. Elec*. 2012, **13**, 273.

31 a) Y. Yang, J. Zhang, Y. Zhou, G. Zhao, C. He, Y. Li, M. Andersson, O. Ingans, F. Zhang, *J.*

Phys. Chem. C. 2010, **114**, 3701; b) A. P. Zoombelt, M. Fonrodona, M. G. R. Turbiez, M. M. Wienk, R. A. J. Janssen, *J. Mater. Chem*. 2009, **19**, 5336.

32 Z. He, C. Zhong, S. Su, M. Xu, H. Wu, Y. Cao, *Nat. Photo*. 2012, **6**, 591.

33 W. Li, K. H. Hendriks, W. S. C. Roelofs, Y. Kim, M. M. Wienk, R. A. J. Janssen, *Adv. Mater*. 2013, **25**, 3182.

34 a) Q. Shi, P. Cheng, Y. Li, X. Zhan, *Adv. Mater*. 2012, **2**, E63; b) J. D. Zimmerman, X. Xiao, C. K. Renshaw, S. Wang, V. V. Diev, M. E. Thompson, S. R. Forrest, *Nano. Lett*. 2012, **12**, 4366.

35 a) R. Fitzner, C. Elschner, M. Weil, C. Uhrich, C. Körner, M. Riede, K. Leo, M. Pfeiffer, E. Reinold, E. M. -Osteritz1, P. Bäuerle, *Adv. Mater*. 2012, **24**, 675; b) Y. –C. Huang, C. –S. Tsao, C. –M. Chuang, C. –H. Lee, F. –H. Hsu, H. –C. Cha, C. –Y. Chen, T. –H. Lin, C. –J. Su, U. –S. Jeng, W. –F. Su, *J. Phys. Chem. C*. 2012, **116**, 10238.

36 I. Osaka, M. Shimawaki, H. Mori, I. Doi, E. Miyazaki, T. Koganezawa, K. Takimiya, *J. Am. Chem. Soc*. 2012, **134**, 3498.

37 M. T. Dang, L. Hirsch, G. Wantz, J. D. Wuest, *Chem. Rev*. 2013, **11**, 3734.

38 a) A. T. Yiu, P. M. Beaujuge, O. P. Lee, C. H. Woo, M. F. Toney, J. M. Frechet, *J. Am. Chem. Soc*. 2012, **134**, 2180; b) H. –Y. Chen, J. Hou, A. E. Hayden, H. Yang, K. N. Houk, Y. Yang, *Adv. Mater*. 2010, **22**, 371.

† **Electronic supplementary information (ESI) available.** See DOI:~

Acknowledgements

This work was supported by the New & Renewable Energy of the Korea Institute of Energy Technology Evaluation and Planning (KETEP) grant funded by the Korea government Ministry of Knowledge Economy (No. 20123010010140)

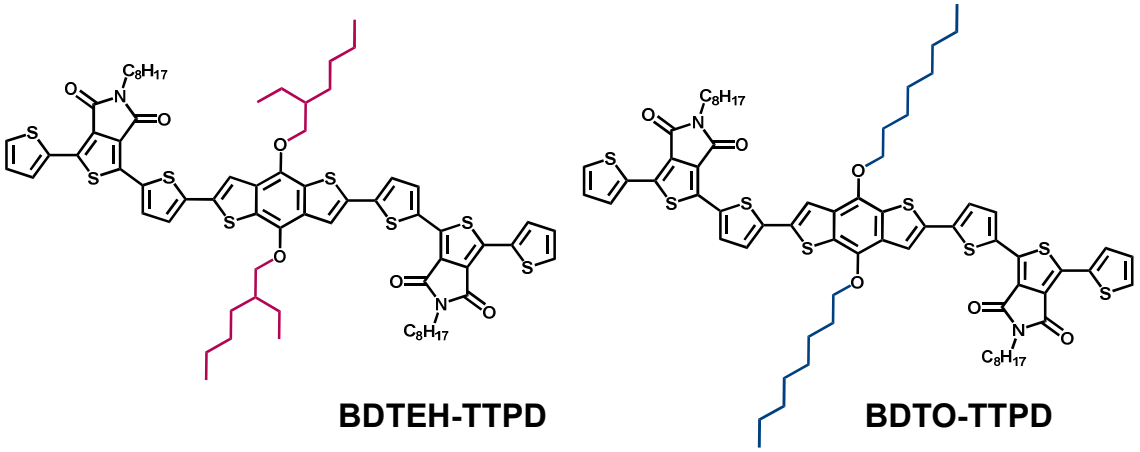

Scheme 1. Molecular structures of the **BDTEH-TTPD** and **BDTO-TTPD** small molecules investigated in this study.

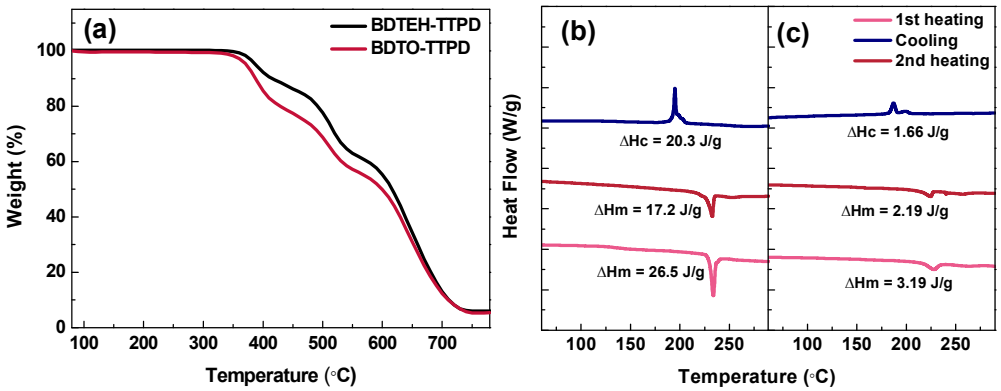

Figure 1. TGA thermograms (a) and DSC curves for **BDTEH-TTPD** (b) and **BDTO-TTPD** (c) recorded under a nitrogen atmosphere at a heating rate of 10 °C/min.

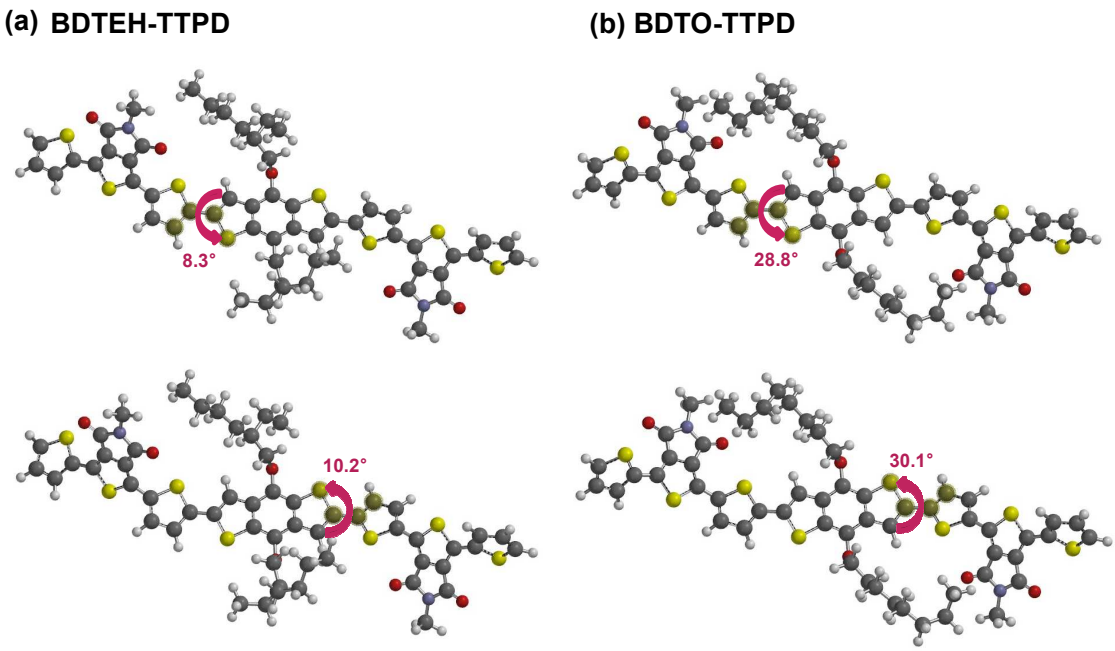

Figure 2. The calculated optimized ground state geometry (a) **BDTEH-TTPD** and (b) **BDTO-TTPD**.

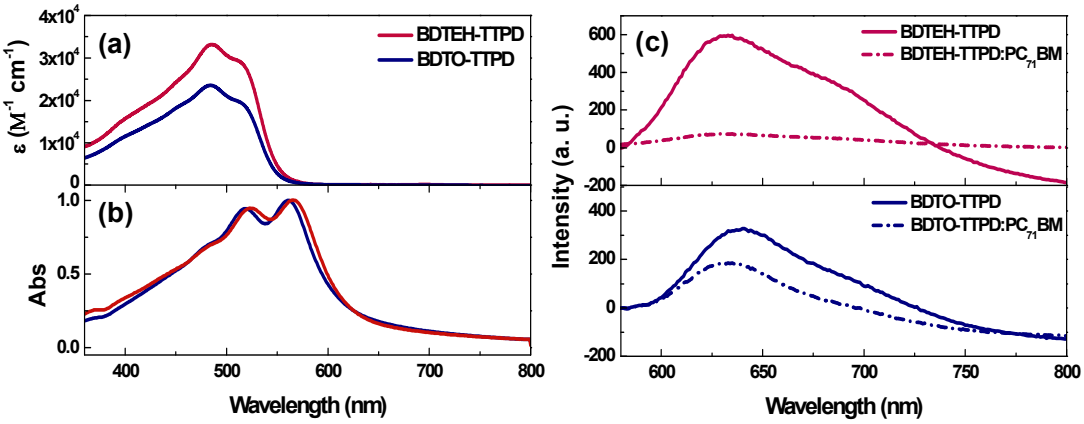

Figure 3. UV-Vis absorption spectra of **BDTEH-TTPD** and **BDTO-TTPD** (a) in chloroform solution (1×10^{-5} M) and (b) in spin-cast films; (c) Photoluminescence spectra of **BDTEH-TTPD**, **BDTO-TTPD**, **BDTEH-TTPD**:$PC_{71}BM$ and **BDTO-TTPD**:$PC_{71}BM$ films.

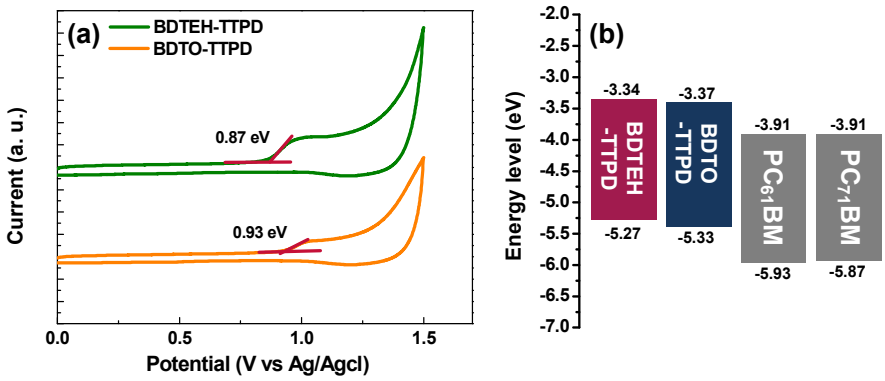

Figure 4. (a) Cyclic voltammograms of **BDTEH-TTPD** and **BDTO-TTPD** spin-cast films and (b) the HOMO and LUMO energy levels of **BDTEH-TTPD**, **BDTO-TTPD**, **$PC_{61}BM$** and **$PC_{71}BM$**.

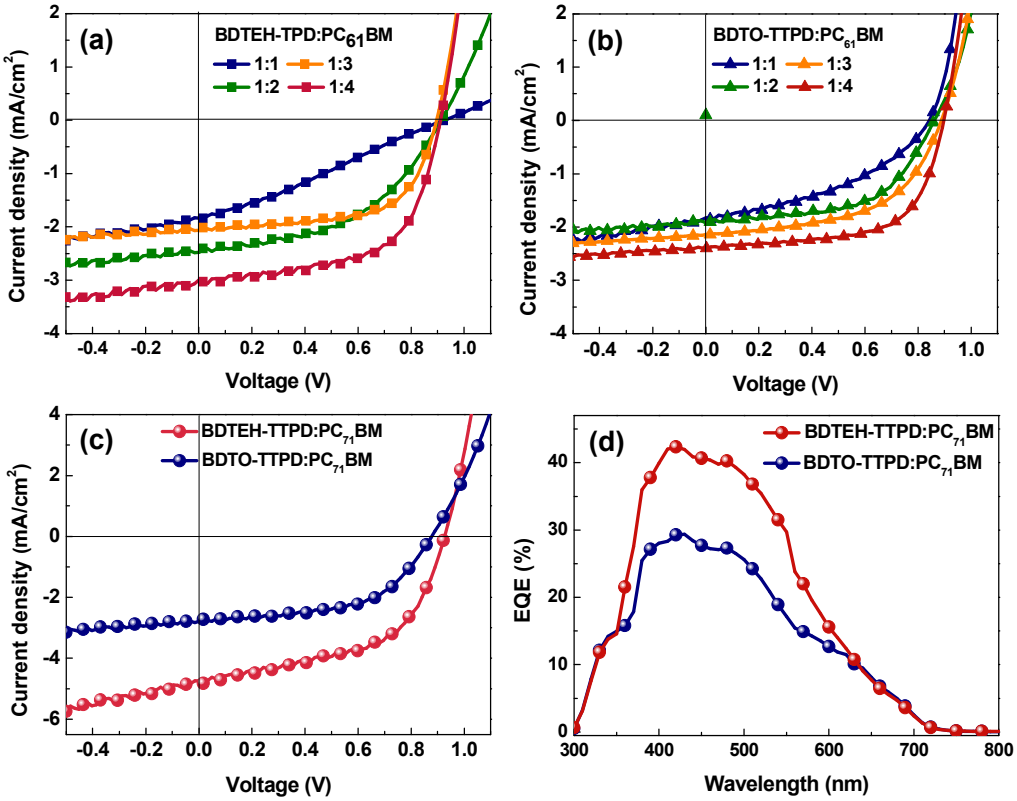

Figure 5. *J-V* curves for solar cell devices based on (a,b) small molecule:$PC_{61}BM$ blends and (c) small molecule:$PC_{71}BM$ blends at a 1:4 weight ratio. (d) EQE spectra of solar cell devices based on small molecule:$PC_{71}BM$ blends.

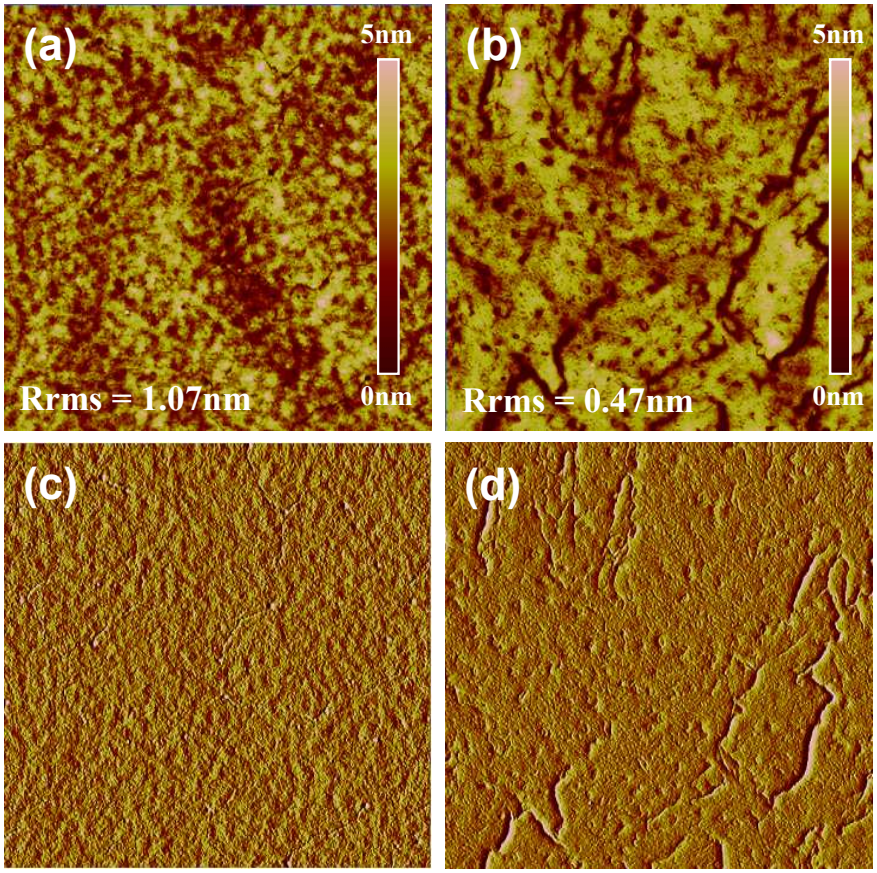

Figure 6. AFM images (5 μm × 5 μm) (first row: height image; second row: phase image) of blend films spin-cast from a chlorobenzene solution: (a-c) **BDTEH-TTPD**:$PC_{71}BM$ (1:4 w/w) and (b-d) **BDTO-TTPD**:$PC_{71}BM$ (1:4 w/w) in tapping mode.

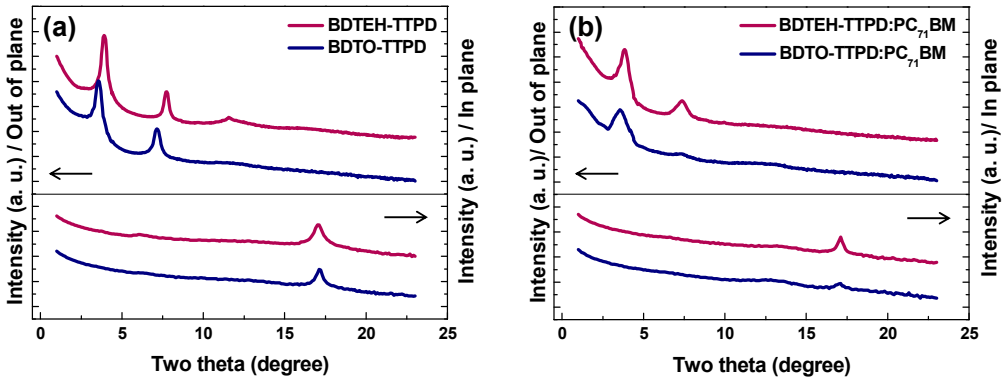

Figure 7. Out-of-plane and in-plane XRD patterns of films of (a) pure **BDTEH-TTPD** (red line) and pure **BDTO-TTPD** (blue line); and (b) blend films (1:4 w/w) of **BDTEH-TTPD**:$PC_{71}BM$ (red line) and **BDTO-TTPD**:$PC_{71}BM$ (blue line).

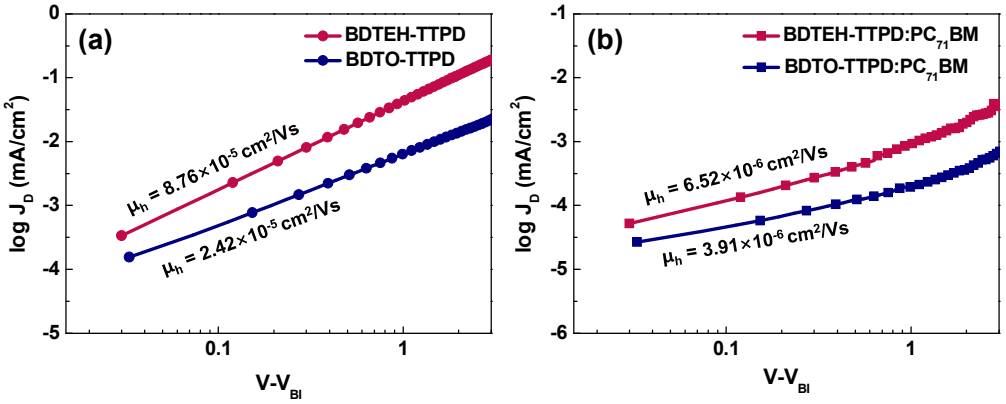

Figure 8. Dark *J-V* characteristics of small molecule (a) and small molecule:$PC_{71}BM$ (b) with hole-only devices.

Table 1. Photophysical properties of the small molecules containing BDT and TPD.

Molecule	T_d (°C) [a]	T_m (°C) [b]	T_c (°C) [c]	λ_{max} (nm) solution	$\varepsilon_{max}/10^3$ solution	λ_{max} (nm) film	λ_{onset} (nm) film	E_g^{opt} (eV) [d]
BDTEH-TTPD	390	234	195	486	33.260	523, 566	642	1.93
BDTO-TTPD	372	228	187	484	23.570	518, 560	631	1.96

[a] Decomposition temperature corresponding to 5% weight loss in N_2 determined by TGA.
[b] Melting temperature determined from DSC.
[c] Crystallization temperature determined from DSC.
[d] Estimated from the absorption edge in film ($E_g^{opt} = 1240/\lambda_{onset}$ eV).

Table 2. Electrochemical properties of the two small molecules.

Compound	E_{onset}^{ox} (eV)	E_{HOMO} (eV)	E_{LUMO} (eV)[a]
BDTEH-TTPD	0.87	-5.27	-3.34
BDTO-TTPD	0.93	-5.33	-3.37

a Calculated using the optical band gap and HOMO energy level of the small molecules.

Table 3. Summary of the photovoltaic data of OSCs based on **BDTEH-TTPD**:PCBM and **BDTO-TTPD**:PCBM blends with different weight ratios.

Small molecule : PCBM	Blend ratio	*V*oc (V)	*J*sc (mA / cm^2)	FF (%)	PCE (%)
BDTEH-TTPD : $PC_{61}BM$	1:1	0.92	1.8	28.0	0.47
	1:2	0.92	2.5	47.1	1.11
	1:3	0.90	2.1	62.5	1.23
	1:4	0.90	3.0	61.1	1.71
BDTEH-TTPD : $PC_{71}BM$	1:4	0.92	4.7	54.4	2.40
BDTO-TTPD : $PC_{61}BM$	1:1	0.86	1.8	42.6	0.65
	1:2	0.87	2.0	56.1	0.97
	1:3	0.88	2.1	54.9	1.02
	1:4	0.87	2.3	55.7	1.10
BDTO-TTPD : $PC_{71}BM$	1:4	0.89	2.7	55.2	1.33